Comparison of Track Topologies of Permanent Magnet Electrodynamic Suspensions

Louis Beauloye
Institute of Mechanics, Materials and Civil Engineering
UCLouvain
Louvain-La-Neuve, Belgium
louis.beauloye@uclouvain.be

Bruno Dehez
Institute of Mechanics, Materials and Civil Engineering
UCLouvain
Louvain-La-Neuve, Belgium
bruno.dehez@uclouvain.be

***Abstract*—High-speed MAGLEV can rely on electrodynamic suspensions for their levitation. The track, the conductive part of the suspension where eddy currents take place, has a great influence on the forces generated in the system. Different track topologies, either discrete or continuous, have been explored so far, but not globally compared. The paper aims therefore to compare objectively continuous and discrete track topologies based on performance criteria such as the lift-to-drag and lift-to-weight ratios.**

Keywords—Maglev, permanent magnet, electrodynamic suspension, track

I. Introduction

Electrodynamic suspensions (EDSs) are considered for the magnetic levitation of high-speed ground transportation systems. They rely on electromagnetic interactions between a magnetic field source and eddy currents induced in a conductive rail by the said source. The former can be realized with permanent magnets (PMs) to generate the magnetic field in a robust and simple way. The latter, also referred as track, can be either discrete or continuous [1]. Continuous tracks are materialized by a homogeneous conductive sheet whereas discrete tracks are formed by the repetition, at regular intervals, of a conductive element that can be made of wire, bulk material, or a combination of both. Several topologies have been considered so far to implement this track, with simple loops, null-flux loops or a ladder; each one having its advantages for specific applications. However, there is no comprehensive global comparison between all of them as well as with continuous tracks. Only topology-to-topology comparisons have been made [2-4].

In this context, the goal of this paper is to compare the continuous and discrete track topologies with relevant performance criteria. First, the track topologies are presented as well as the selected performance criteria. Then, the models are developed. A bi-objective optimization is conducted in Section IV. Finally, the track topologies are compared based on the optimization results in Section V.

II. PM-EDS Topologies and Criteria

A. Magnetic field source

The magnetic field source of PM-EDS is an arrangement of PMs in a Halbach array or with a simple alternance of poles. The latter is chosen for this study and remains the same for all the track topologies.

B. Track topologies

The different track topologies used in this paper are represented in Fig. 1. Topologies (SL)-(LA) are discrete while the first one (PL) is continuous. The levitation and motion directions are along the y-axis and x-axis respectively.

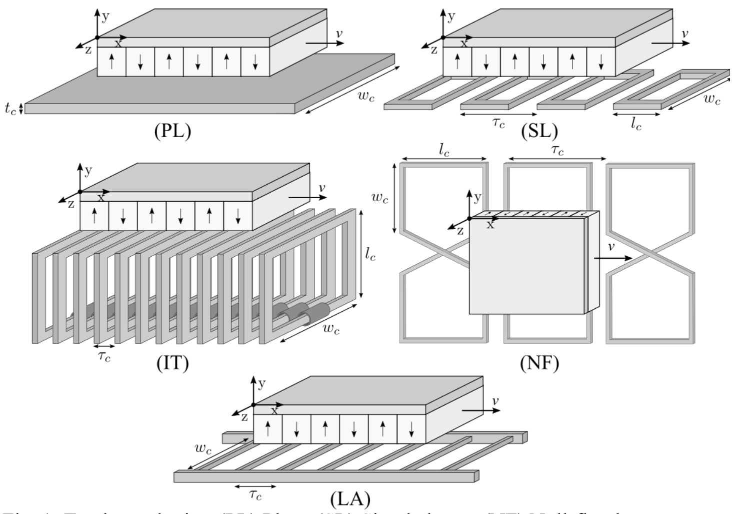

Fig. 1: Track topologies. (PL) Plate. (SL) Simple loops. (NF) Null-flux loops. (IT) Inductrack1 [6]. (LA) Ladder.

C. Criteria

The criteria used for the comparison are the following:

- Lift-to-drag ratio (LDR): the ratio between the lift force and the drag force.
- Lift-to-weight ratio (LWR): the ratio between the lift force and the weight of the PMs of the source.

III. Modelling

Different types of model have to be used to compute the forces in the continuous and in the discrete tracks [1]. These models are developed in this section for each topology. The equivalent circuits model of the discrete tracks are similar to the ones in [3, 7]. The forces can be derived based on the currents in the circuits using either the magnetic co-energy or the Lorentz force equation. There are two main hypotheses behind this model. First, the currents induced locally in the conductors are neglected, meaning that the wire cross section should not be too large. Secondly, the geometry is supposed to be infinite along the x-axis. The circuits for each topology are depicted in Fig. 2.

A. Plate

The forces in the continuous track are computed using a 3D analytical model as in [5], starting from local formulations of Maxwell equations. The geometry is decomposed in regions that are either air, PM or electrical conductor.

In the air, the following equation holds:

$$\nabla^2 \phi = 0 \quad (1)$$

where ϕ is the magnetic scalar potential.

L.Beauloye is a Research Fellow of the Fonds de la Recherche Scientifique (FNRS).

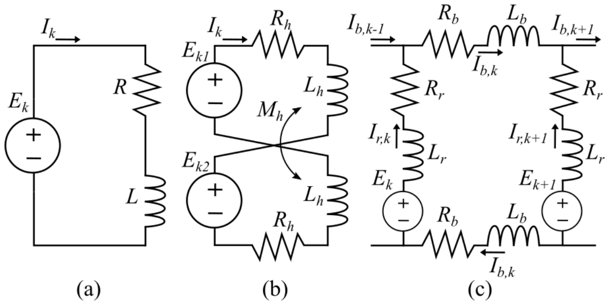

Fig. 2: Equivalent circuits for (a) the simple loops and Inductrack1, (b) null-flux loops and (c) ladder topologies.

In the PMs:

$$\nabla^2 \phi = \nabla \cdot \boldsymbol{M} \quad (2)$$

where $\boldsymbol{M}$ is the residual magnetization vector of the PMs.

In the conductor:

$$\boldsymbol{\nabla}^2 \boldsymbol{H} = -\sigma \mu_0 \boldsymbol{\nabla} \times (\boldsymbol{v} \times \boldsymbol{H}) \quad (3)$$

where $\mathbf{H}$ is the magnetic field strength, σ is the electrical conductivity and $\boldsymbol{v}$ is the speed of the vehicle.

The forces are then computed using Maxwell's stress tensor.

B. Simple Loops

The discrete tracks are modeled using an equivalent circuit governed by the following equation [7]:

$$RI_0 + L\frac{dI_0}{dt} + \sum_{k=1}^{N} M_k \left(\frac{dI_{-k}}{dt} + \frac{dI_k}{dt}\right) - E_0 = 0 \quad (4)$$

where R and L are the resistance and inductance of the loops, M_k is the mutual inductance between the k-th loop and the center loop (0-th), E_0 is the voltage induced in the center loop due to the variation of the magnetic flux intercepted by this loop, and $2N$ is the number of adjacent loops considered along the x-axis. The current and the voltage can be written as Fourier series with the same spatial frequency depending on the pole pitch of the PMs:

$$I_k = \sum_{n}^{N_h} I_{kn}\, e^{j\omega_n x}\ , \qquad E_k = \sum_{n}^{N_h} E_{kn}\, e^{j\omega_n x} \quad (5)$$

with $\omega_n = \frac{n\,\pi}{\tau_m}$ and τ_m the PM pole pitch, and N_h the number of harmonics. For each harmonic, the electrical equation can be then expressed as:

$$RI_{0n} + v_x j\omega_n L I_{0n} + v_x \sum_{k=1}^{N} j\omega_n M_k (I_{-kn} + I_{kn}) - E_{0n} = 0 \quad (6)$$

Since the currents are periodic, an equivalent inductance can be computed as:

$$L_{en} = L + \sum_{k} 2\, M_k \cos(k\omega_n \tau_c) \quad (7)$$

where τ_c is the coil pitch.

Finally, the current in the k-th loop is computed in the following way:

$$i_k = Re\left\{\sum_{n} \frac{E_{kn}}{R + v_x j\omega_n L_{en}}\ e^{j\omega_n (x + k\tau_c)}\right\} \quad (8)$$

For the simple loops topology, E_{kn} is equal to:

$$E_{kn} = -v_x \frac{\partial}{\partial x}\left(\int_{x-l_c/2}^{x+l_c/2} \int_{-\frac{w_c}{2}}^{\frac{w_c}{2}} B_{yn}(x', y, z)\, dy dx' \right) \quad (9)$$

with w_c and l_c the width and the length of the loops respectively, and B_{yn} the n-th harmonic of the y-component of PM magnetic flux density computed with a model similar to the one describe above.

C. Inductrack 1

The equations are the same for the Inductrack 1 as (8), except that:

$$E_{kn} = -v_x \frac{\partial}{\partial x}\left(\int_{0}^{l_c} \int_{-\frac{w_c}{2}}^{\frac{w_c}{2}} B_{xn}(x, y, z)\, dy dz \right) \quad (10)$$

D. Null-flux loops

The equations are the same for the null-flux loops as (8), except that $R = 2\,R_h$, $L = 2\,(L_h - M_h)$, and $E_k = E_{k1} - E_{k2}$ where $E_{k1,2}$ are computed similarly as (9).

E. Ladder

In the ladder track, all the loops are electrically interconnected. Therefore, to compute the currents in the rungs I_r and in the bars I_b of the ladder, two equations are required:

$$(R_r + v_x j\omega_n L_{re}) I_{rkn} (1 - e^{j\omega_n \tau_c}) + 2(R_b + v_x j\omega_n L_{be}) I_{bkn} - E_{kn}(1 - e^{j\omega_n \tau_c}) = 0 \quad (11)$$

$$I_{rk} + I_{bk} e^{-j\omega_n \tau_c} = I_{bk} \quad (12)$$

with

$$E_{kn} = \int_{-\frac{w_c}{2}}^{\frac{w_c}{2}} \boldsymbol{v} \times \boldsymbol{B_n}\, dz \quad (13)$$

F. Multiple conductor tracks

For the simple loops, Inductrack 1 and the null-flux loops, each loop can be made of a plurality of turns. In this case, the conductors in these types of track are discretized in several turns and the magnetic flux is computed on each turn. For the ladder track, the rungs can be divided in several parallel conductors, requiring additional voltage Kirchhoff laws between pairs of adjacent conductors in each rung.

G. FEM validation

All the models were validated with FEM simulations in COMSOL Multiphysics. Fig. 3 depicts the forces computed with three different models for a velocity of 10m/s. It should be noted that, at this speed, the skin effect is negligible in the conductors. The temporal model is obtained from a temporal integration of the electrical equations. The discrepancy between the three models is very small.

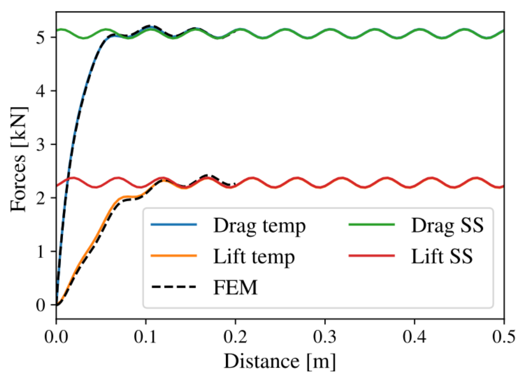

Fig. 3: Comparison between the steady-state (SS) model, an analytical transient analysis (temp), and FEM for the ladder track at 10 m/s.

IV. Optimization

The five topologies are optimized based on the developed models and can then be fairly compared. The optimization relies on a bi-objective maximization using the algorithm NSGA-III where the objectives are the comparison criteria defined above. The forces involved in the objectives are computed for one wavelength of the magnetic field source.

The parameters of the PM-EDSs are presented in Table I. Some design choices must be noted. In the simple loops (SL) and null-flux loops (NF) topologies, the gap between adjacent loops is chosen to be minimal. The levitation height of the PMs in front of the null-flux loops (NF) is set to 1/4 of the loops width to ensure a sufficient lift force at the expense of a reduction of the LDR. There is no inductive loading at the bottom of the Inductrack (IT). The width of the plate (PL) is set to 3 times the width of the PMs to remain in the validity area of the model. The conductors in the discrete tracks have a cross-section equal to:

$$A_c = (N_t \times w_{tc}) \times (N_l \times w_{lc}) \quad (14)$$

The optimization parameters and their range of values are summarized in Table II. The thickness of the plate t_c depends on the skin depth δ_{skin}. The numbers of turns are not optimized in the ladder track (LA). Indeed, we observed that the optimization tended to maximize these parameters, towards the limits of the model. Since the current in each conductor making a rung is different, it is more complex to consider the coupling between them. A more comprehensive model needs therefore to be developed to go further. However, the ladder with only one turn remains an interesting topology to study and to compare with the other ones.

V. Results and Comparison

The Pareto fronts between the LWR and LDR obtained after the optimization of the parameters with a PM pole pitch equal to 0.2 m are shown in Fig. 4. Several key points are noted on the graph and their metrics reported in Table III. The resulting suspensions are represented in Fig. 5 to visualize the optimum dimensions and the differences between them. The first line is a view from above the PMs and the second one a cut-view perpendicular to the direction of travel.

TABLE I. PM-EDS Parameters

Parameter	Symbol	Value	Unit
Pole pitch of the PMs	τ_m	0.2	m
Width of the PMs	w_m	$2\ \tau_m$	m
Thickness of the PMs	t_m	$\tau_m/4$	m
Remanence of the PMs	B_r	1.4	T
Air gap thickness	τ_{ag}	30	mm
Coil pitch	τ_c	-	m
Width of the track	w_c	-	m
Length of the loops	l_c	-	m
Number of turns in the thickness of the loops	N_t	-	-
Number of turns in the length of the loops	N_l	-	-
Wire cross section	$w_{tc} \times w_{lc}$	10×10	mm^2
Thickness of the plate	t_c	-	m
Electrical conductivity	σ	3.5e7	S/m
Translational speed	v_x	100	m/s

TABLE II. Optimization Parameters

Topology	Parameter	Min	Max
PL	t_c	$\delta_{skin}/10$	$3\ \delta_{skin}$
SL	τ_c/τ_m	0.1	1
	w_c/w_m	0.5	3
	N_l	1	10
	N_t	1	10
IT	τ_c/τ_m	0.05	1
	w_c/w_m	0.5	3
	l_c	0.05	0.5
	N_l	1	20
	N_t	1	10
NF	τ_c/τ_m	0.1	1
	w_c/w_m	0.5	3
	N_l	1	10
	N_t	1	10
LA	τ_c/τ_m	0.1	1
	w_c/w_m	0.5	3

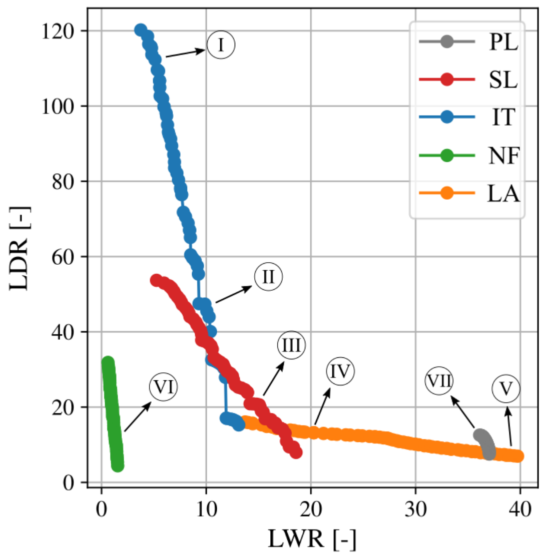

Fig. 4: Pareto fronts after optimization of the five track topologies.

TABLE III. Optimization Results

PM-EDS	Topology	LWR [-]	LDR [-]	Track volume [m^3]
I	IT	5.1	112.3	0.053
II	IT	10.3	44	0.014
III	SL	13.7	24.6	0.003
IV	LA	20.2	13.2	0.0027
V	LA	38.7	7.2	0.0017
VI	NF	1.24	13.7	0.0044
VII	PL	36.2	12.5	0.0038

For each topology, there is a trade-off between LDR and LWR. The null-flux topology (NF) is dominated by all the other ones. When using PMs instead of superconductors, the magnetic flux intercepted by the null-flux loops is too low compared to the weight of the source. The Inductrack1 (IT) can reach a very high LDR but a rather low lift force while the ladder track (LA) can produce a much more significant lift force but a poor LDR. The simple loops (SL) can be a

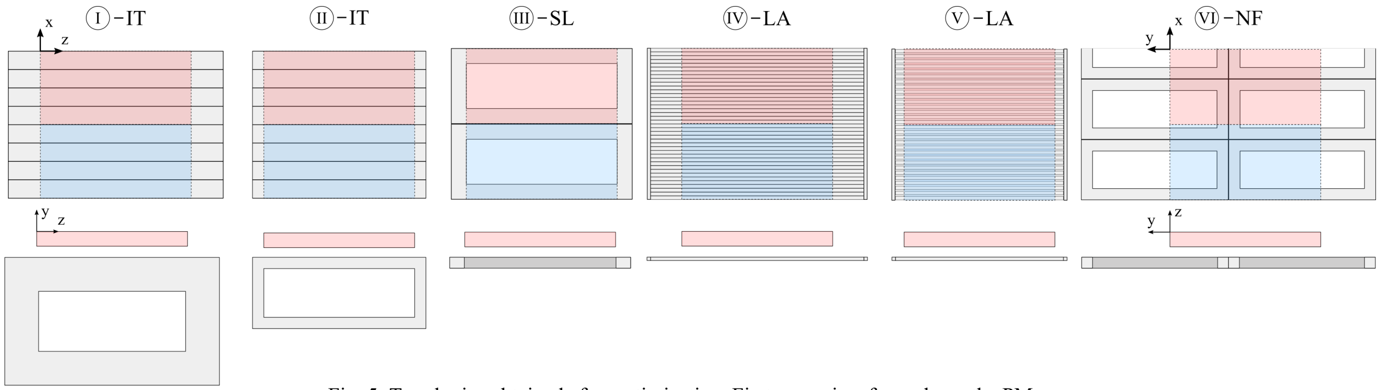

Fig. 5: Topologies obtained after optimization. First row: view from above the PMs.
Second row: Cut-view perpendicular to the direction of motion.

trade-off between the two with a slight improvement of the extreme points of both previous topologies. However, the simple loops (SL) requires much less materials than the Inductrack1 (IT) for the same performance which can reduce significantly the costs. The ladder (LA) can also be cost-efficient with the lowest amount of material for the largest lift force. Despite one of the lowest LDR, the conductive plate (PL) still produces a high LWR, above 35, leading to a lower PM cost for a given application. It also has a rather small track volume and a much easier building process compared to the other topology. These two elements could lead to a significantly lower initial cost of the suspension but this has to be compared to the higher operation cost due to the low LDR. Finally, the ladder track (LA) could reach better performance with more conductors per rung but this still has to be proven with a more comprehensive model.

It is important to assess the validity of the comparison with the variation of parameters such as the speed, the PM pole pitch or the wire section. The LWR will not increase with the speed since the lift force saturates while the speed increases. However, the LDR will change with the speed. As the LDR is proportional to the speed for all the discrete tracks, the comparison between them will remain unchanged. Only, the plate track will have a smaller LDR relatively to the others because its LDR increases with the square root of the speed. Fig. 6 shows the influence of the pole pitch of the PM on the Pareto fronts. It can be seen that with a pole pitch two times longer, the conclusions drawn earlier remain valid. Finally, with a wire section four times smaller, the Pareto fronts of the Inductrack, the simple loops, and the null-flux loops are almost the same as before in Fig. 7. This shows that, as long as the wire cross-section remains relatively small, it has almost no influence on the forces. This result also validates the models with discretized conductors.

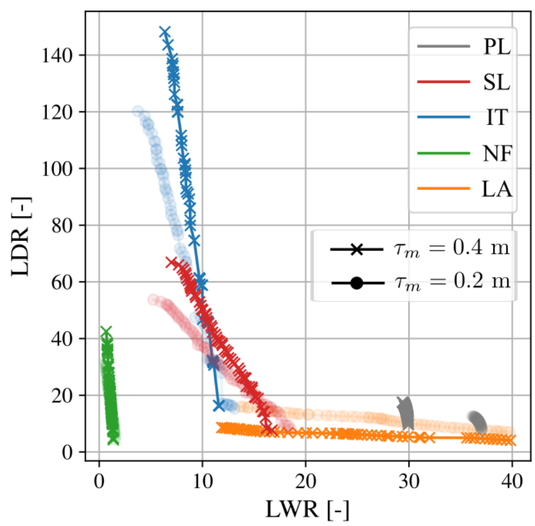

Fig. 6: Pareto fronts after the optimization of the tracks with two different PM pole pitches.

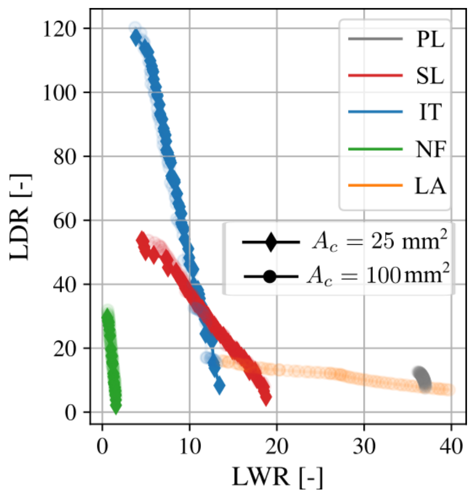

Fig. 7: Pareto fronts after the optimization of the tracks with two different wire cross-sections.

VI. Conclusion

This paper compared five different track topologies of permanent magnet electrodynamic suspension. To accomplish this, the tracks were modelled using analytical models. Based on this, a bi-objective optimization was performed to extract Pareto fronts between lift-to-drag and lift-to-weight ratios for each topology. It was then shown that the PM-EDS with null-flux coils have poor performance compared to the others. The Inductrack1 can reach a very high LDR while the ladder track a high LWR. The topology with simple non-connected loops sits in-between these two. Thanks to a high LWR, a small track volume and cheaper construction cost, the plate track could be a very cost-effective topology, at least initially. When taking the operation cost into consideration, this could be mitigated. Finally, the robustness of these conclusions was tested against the variation of other design parameters.

REFERENCES

[1] L. Beauloye and B. Dehez, "Permanent Magnet Electrodynamic Suspensions Applied to MAGLEV Transportation Systems: A Review", *IEEE Transactions on Transportation Electrification*, vol. 9, no. 1, pp. 748-758, March 2023.

[2] T. Akinbiyi, P. Burke, and B. Ooi, "A comparison of ladder and sheet guideways for electrodynamic levitation of high speed vehicles," *IEEE Trans. Magn.*, vol. 12, no. 6, pp. 879–881, Nov. 1976.

[3] Yu Ju Chen and Jun Feng, "Optimization of guideway coil dimensions for a magnetic levitation system," *IEEE Trans. Magn.*, vol. 33, no. 5, pp. 4335–4344, Sep. 1997.

[4] Guo, Li, and Zhou, "Study of a Null-Flux Coil Electrodynamic Suspension Structure for Evacuated Tube Transportation," *Symmetry*, vol. 11, no. 10, p. 1239, Oct. 2019.

[5] S. Tongyu and W. Dazhi, "3D Analytical model of drag and lift force for a conductive plate moving above a Halbach magnet array," *Transactions of the Institute of Measurement and Control*, vol. 40, no. 12, pp. 3515–3524, Aug. 2018.

[6] R. F. Post and D. D. Ryutov, "The inductrack: A simpler approach to magnetic levitation," *IEEE Trans. Appl. Supercond.*, vol. 10, no. 1, pp. 901–904, Mar. 2000.

[7] J. Lim *et al.*, "Equivalent inductance model for the design analysis of electrodynamic suspension coils for hyperloop," *Sci Rep*, vol. 11, no. 1, p. 23499, Dec. 2021.